processes

MDPI

Article

A Numerical Simulation Investigation on the Distribution Characteristics of Coal Seam In Situ Stress Under the Influence of Normal Fault

Zhihua Rao [1,*], Qingjie Du [1], Chunsheng Xiang [1], Zhongying Han [2] and Yanbo Liang [2]

[1] CNOOC China Ltd., Shenzhen 518054, China; duqj2@cnoooc.com.cn (Q.D.); xiangchsh@cnoooc.com.cn (C.X.)
[2] School of Petroleum Engineering, China University of Petroleum (East China), Qingdao 266580, China; hanzhying@upc.edu.cn (Z.H.); b20020011@s.upc.edu.cn (Y.L.)
* Correspondence: raozhh@cnoooc.com.cn

Abstract: This study focuses on the complex stress distribution in coal seams influenced by normal fault using the fault development zone of the LF-M1 oilfield in southern China as a case study. Based on 3D seismic and drilling data, a key research area was delineated, and strata were reclassified considering rock parameter similarity. An FLAC3D model encompassing hanging wall, normal fault, and footwall strata was developed to systematically analyze geostress near the fault under various conditions. The results indicate that the normal fault induces non-uniform and discontinuous stress patterns in the coal seam's transverse plane. Stress weakening occurs near the fault, with a pronounced concentration on its flanks, approaching in situ stress levels in the far field. Coal's Poisson's ratio, elastic modulus, and fault dip negatively correlate with horizontal in situ stress, whereas other parameters show positive correlations. The maximum horizontal stress is more sensitive to parameter variations than the minimum. Stress weakening is most influenced by coal's Poisson's ratio, followed by coal's elastic modulus, fault elastic modulus, fault Poisson's ratio, fault dip, and fault thickness and the coal seam thickness. Notably, a 20% decrease in coal's Poisson's ratio leads to a 23.32% stress reduction at measuring point 1. Conversely, the coal seam thickness has a minimal impact on stress across the fault. When the coal seam thickness increases by 20%, the maximum horizontal stress at measuring point 2 only decreases by 0.06%. In summary, fault geometry, rock mechanics parameters, and external loads collectively complicate stress distributions near faults, posing risks of drilling accidents such as wellbore instability, leakage, and reservoir damage, necessitating careful consideration.

Keywords: normal fault; coal seam; in situ stress; numerical simulation; sensitivity analysis

check for updates

Academic Editor: Zheng Sun

Received: 27 December 2024
Revised: 6 February 2025
Accepted: 12 February 2025
Published: 14 February 2025

Citation: Rao, Z.; Du, Q.; Xiang, C.; Han, Z.; Liang, Y. A Numerical Simulation Investigation on the Distribution Characteristics of Coal Seam In Situ Stress Under the Influence of Normal Fault. *Processes* **2025**, *13*, 538. https://doi.org/10.3390/pr13020538

Copyright: © 2025 by the authors. Licensee MDPI, Basel, Switzerland. This article is an open access article distributed under the terms and conditions of the Creative Commons Attribution (CC BY) license (https://creativecommons.org/licenses/by/4.0/).

1. Introduction

The study of in situ stress involves multiple fields of engineering construction, such as oil and gas exploration and development [1,2], mining [3,4], tunnel construction, earthquake prediction, and hydropower engineering [5,6]. Fully understanding the distribution characteristics of in situ stress in the construction area can help improve the safety of engineering construction. Due to the influence of geological activities and human construction, there are often numerous joints, fissures, and faults developed in the strata, highlighting the heterogeneity and discontinuity characteristics of the strata [7,8]. When drilling encounters unstable areas such as faults, the distribution of in situ stress becomes complex, and there are often uneven stress distribution and stress direction torsion, which increase

risks in construction. Furthermore, the presence of weak coal seams in proximity to faults exacerbates the stress complexity, frequently resulting in drilling hazards such as wellbore instability and collapse. Consequently, a comprehensive and systematic understanding of coal seam stress distribution in faulted zones is crucial [9–12].

At present, numerous researchers have conducted extensive research on the distribution of in situ stress, especially in the vicinity of faults, using theoretical analysis, on-site measurements, indoor experiments, and numerical simulations. In terms of on-site testing, there are various measurement methods, mainly including the hydraulic fracturing testing method, stress release method, microseismic method, acoustic emission method, etc. Li et al. used 168 sets of hydraulic fracturing testing data and overcooling data combined with 84 sets of earthquake focal mechanism solutions to study the distribution of in situ stress and the stability of fault areas near Beijing, China [13]. Li et al. used an improved overcooling technique to study the distribution characteristics of in situ stress and the relationship between faults in the central mining area of China, which overcome the limitations of previous data scarcity and dispersion [14]. Li et al. also conducted an analysis of the current geostress field surrounding the Yishu fault zone in eastern China, unveiling the intricate stress state in its vicinity and furnishing vital guidance for engineering designs within the region [15]. Yuan et al. used the hydraulic fracturing testing method to measure in situ stress at different distances near the Xianshuihe fault zone in southwestern China and obtained the overall in situ stress distribution characteristics of the tunnel construction area through multiple linear regression to guide tunnel construction in the area [16]. On the basis of summarizing the advantages and disadvantages of different stress testing methods, Ji et al. utilized the stress relief method of hollow inclusion and measured the distribution characteristics of in situ stress in the 420 m horizontal development roadway of the Gucheng coal mine to guide the optimization and support design of the roadway [17]. Cheng et al. employed the stress release method and stress inversion model to ascertain the stress distribution at the Gaojiapu coal mine, thereby offering insights for the efficient and safe extraction of coal [18]. Yong et al. comprehensively applied multiple diagnostic fracturing injection tests (DFITs) and pressure transient analysis (PTA) to elucidate the horizontal stress and pore pressure distribution patterns within the Longmaxi shale gas field in the Sichuan Basin, China, providing crucial guidance for on-site fracturing production operations [19]. Zhao et al. comprehensively used various methods, such as hydraulic fracturing, stress recovery, and drilling stress measurement, to test the in situ stress of candidate areas for nuclear waste disposal in Xinjiang, which can help guide underground construction stability and optimize facility structure to ensure long-term safety [20]. Roshan et al. proposed a new method for estimating in situ stress, which utilizes borehole deformation analysis techniques to analyze borehole television data to estimate in situ stress [21].

In terms of indoor experiments, researchers mainly conducted research by shrinking the strata according to similar proportions to establish physical models. Jiang et al. established two similar material physical models to investigate the impact of fault activation on mining under various mining directions, discovering that the risk of rock bursts was higher in the fault's lower section compared to the upper strata [22]. Wang et al. also used similar material simulation experiments to study the evolution law of overlying rock stress and rock fracture failure law during coal seam mining under the influence of faults, providing guidance for the stability analysis of coal seam strata [23,24]. Su et al. used similar materials to construct a strike slip fault model in the laboratory and recorded the stress distribution at different positions near the fault by laying stress sensors in the model. The research results reveal the stress distribution characteristics in the area near the strike slip fault, providing a reference for understanding fault activity and earthquake mechanisms under real geologi-

cal conditions [25]. Lin et al. constructed a large-scale, three-dimensional physical model to simulate tunnel excavation in deep strata subjected to high ground stress and pore pressure conditions, studying tunnel deformation and failure mechanisms, and offering valuable insights for tunnel design and support systems [26]. Hao et al. and Feng et al. conducted similar studies and established larger-scale physical model experimental systems, providing new reliable tools for more research on underground engineering construction [27]. In addition, some researchers have conducted small-scale indoor mechanical loading experiments to study the stress distribution and activation mechanism near faults [28]. Ju et al. conducted direct shear experiments on 3D-printed fault models for photoelastic analysis and studied the influence of fault roughness characteristics on the stress evolution characteristics near faults [29]. Giorgetti et al. studied the preparation of sandstone cylinders filled with clay-rich fault mud, conducted triaxial mechanical experiments, and investigated the effect of different fault angles on stress changes. Their research results contribute to a more accurate assessment of the seismic risk of faults, thereby improving the effectiveness of earthquake prevention and disaster reduction [30].

There are many numerical simulation methods for studying in situ stress, including the finite element method (FEM), finite difference method (FDM), and discrete element method (DEM). Yin et al. analyzed the impact of a strike-slip fault in the Qinshui Basin on stress and methane production using a 3D finite element model [31]. Ehtesham et al. used the 3D discrete element software 3DEC to model some fractured rock masses in the North Perth Basin, analyzing stress field disturbances near faults in the model, with a focus on studying the influence of fault properties on in situ stress anisotropy correspondence [32]. Jiang et al. used the two-dimensional discrete element software UDEC to establish numerical models for different coal seam mining sequences and studied the spatiotemporal evolution law of stress in the mining face near the fault, analyzing the instability of the fault [33]. To overcome the limitations of measuring in situ stress in high-stress environments, Ai et al. proposed a slot relief method for performing high-stress in situ stress measurements, validated through simulations and field tests [34]. Xu et al. established a two-dimensional numerical model containing faults, studied the distribution characteristics of coal seam stress under different fault parameters, and combined the numerical simulation results with artificial neural networks to construct a stress field prediction model [35]. Xu et al. also conducted in situ stress inversion based on the results of in situ stress testing combined with the least squares multiple linear regression method, and they applied the inversion results as boundary conditions to a three-dimensional numerical model to obtain the initial stress field distribution in the fault zone [36]. Zhang et al. used the iterative inversion method of boundary stress to study the in situ stress field in deep strata through numerical simulation and analyzed the development characteristics of cracks around faults using the Griffith mathematical model in crack mechanics theory [37]. Kou et al. established a comprehensive three-dimensional numerical model to analyze in situ stress around tunnels, focusing on the influence of the fault type, direction, width, rock bedding direction, elastic modulus ratio of surrounding rock and fault, and principal stress ratio on the stress field [38]. Li et al. used FLAC3D to establish a three-dimensional numerical model of the Gaoyang coal mine in Shaanxi Province, China, as the engineering background and studied the stress evolution and motion law of fault sliding under different fault dip angles, providing guidance for the on-site coal seam in the fault area [39]. He et al. used MIDAS/GTS numerical software to obtain stress and displacement deformation results, focusing on analyzing the formation mechanism of the Xiaoyudong fault with NW trending and exploring its relationship with earthquake occurrence [40].

In summary, on-site stress measurement is complex, costly, and limited in data availability, while indoor experiments with similar materials are constrained by material proper-

ties and simplifications, exhibiting poor repeatability and inadequate simulations of real geological formations. Given the rapid development of numerical simulation technology in recent years, which has seen significant progress in modeling methods and computational solutions, coupled with strong repeatability and economic efficiency, this article aims to establish a numerical model incorporating normal fault based on the LF-M1 structural belt in the LF depression area of southern China. This model will analyze the influence of coal seam and fault physico-mechanical properties on coal seam stress and help conduct a sensitivity analysis to provide theoretical support for on-site drilling operations.

2. Research Background

The LF-M1 structural belt in the LF depression area of southern China was taken as the engineering background. As shown in Figures 1 and 2, through the analysis of on-site 3D seismic results, regional data, and existing drilling data, we identified the LF-M1 block as the priority target for exploitation. The strata in this area are complex, with developed faults, thin coal seams, and diverse rock types, which have brought many challenges to the drilling work. During the drilling process, the LF-M1-1 well was drilled first, and then LF-M1-2 and LF-M1-3 evaluation wells were drilled sideways in the north and south directions. The 3D seismic results show that the LF-M1-1 well encountered fault F2 and a coal seam at 3223 m, while the LF-M1-2 well encountered a coal seam at 3233 m. The coal seam encountered during the drilling of the two wells has a drop of 10 m. Therefore, strata with burial depths in the range of 3200 m to 3260 m were selected for research.

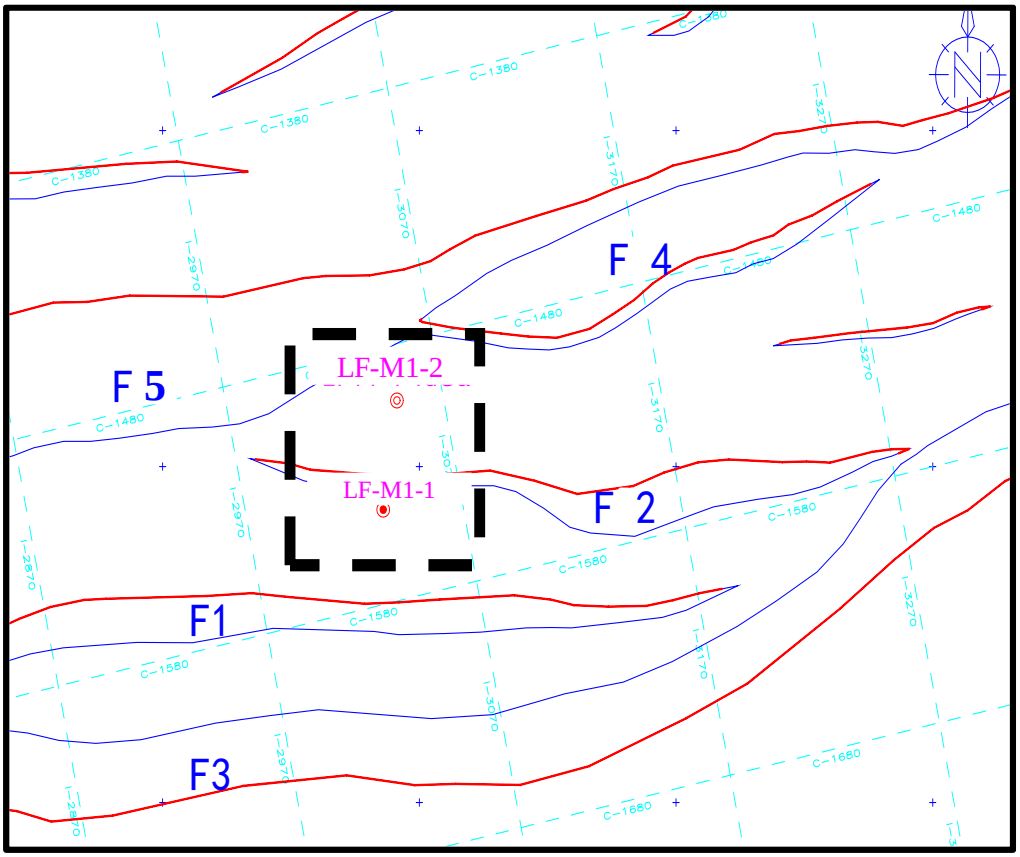


Figure 1. Plane distributive maps of T2 fault in LF M1 oilfield.

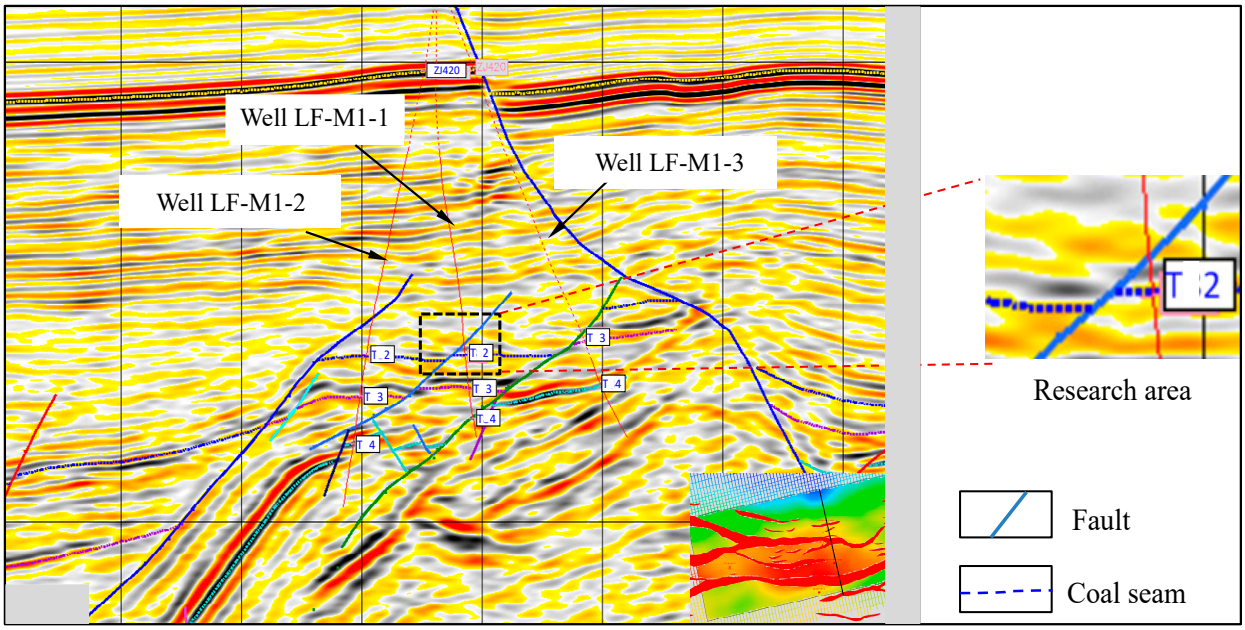


Figure 2. Three-dimensional seismic interpretation profile and study area selection of LF M1 oilfield.

3. Numerical Model

Lithology histograms of the strata obtained from wells LF-M1-1 and LF-M1-2 served as the foundation for selecting the lithologies of the hanging wall and footwall in the model. The rock formations within the study area exhibit diversity in both lithology and thickness. To facilitate the research, the strata were streamlined based on the general principle of amalgamating rock parameters. The strata types in the model were divided into three groups, including fault hanging wall, normal fault, and fault footwall. Except for the fault, all other strata are horizontal and uniformly thick, with a fault thickness of 20 m and a dip angle of 45°. The hanging wall and footwall of the fault contain five types of rocks, including coal rock, mudstone, siltstone, fine sandstone, and medium sandstone, totaling 20 layers. This article uses FLAC3D for simulation, and the specific numerical model is shown in Figure 3. The schematic diagram of rock layer division is shown in Figure 4. The model size is X × Y × Z = 150 m × 50 m × 60 m. The top of the model is buried at a depth of 3200 m, so a rock self-weight stress of 75 MPa is applied at the upper boundary as stress compensation. The maximum horizontal stress is applied on both sides in the X direction, with a lateral pressure coefficient of 0.8. The minimum horizontal stress is applied on both sides in the Y direction, with a lateral pressure coefficient of 0.7. The bottom boundary is fixed. In addition, rock density was obtained through logging data, and the rock elastic modulus and Poisson's ratio were obtained by making standard rock cores and conducting triaxial mechanical experiments. The specific parameter results are shown in Table 1. Considering that this article focuses on the overall study of the distribution of coal seam stress under the condition of fault existence, without considering the excavation of coal seams and fault slip, in order to simplify the calculation, the rock constitutive model chooses an elastic constitutive model, and the rocks are all homogeneous and isotropic media.

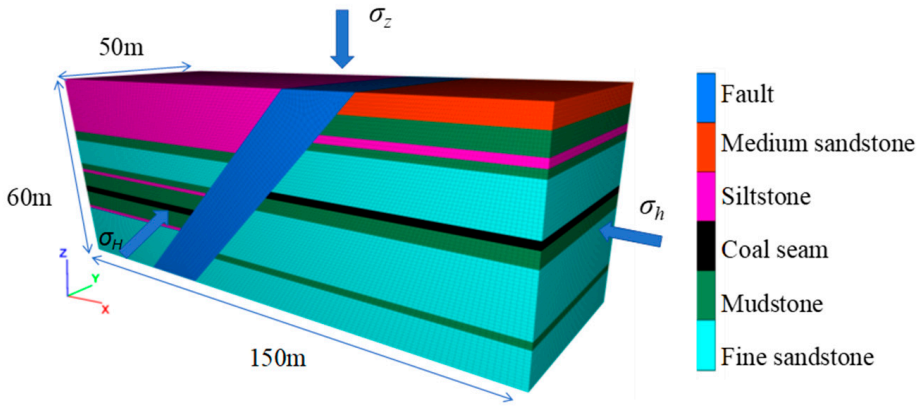


Figure 3. Three-dimensional numerical model diagram.

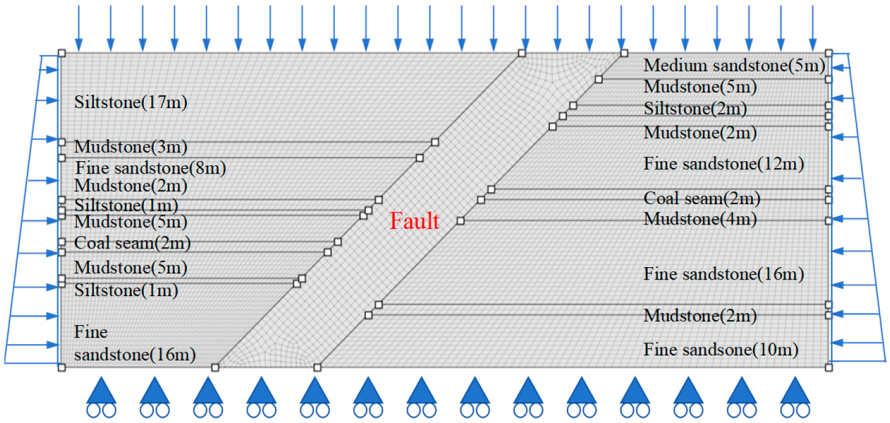


Figure 4. Model boundary conditions and rock layer distribution.

Table 1. Table of physical and mechanical parameters of rock strata.

Strata Group	Lithology	Parameters		
		Density ρ/kg/m^3	**Elastic Modulus E/GPa**	**Poisson's Ratio v**
Hanging wall and footwall	Coal seam	1200	3.73	0.35
	Mudstone	2500	13.3	0.23
	Siltstone	2600	16.8	0.25
	Fine sandstone	2620	14.5	0.22
	Medium sandstone	2650	15.6	0.23
Fault	Weak strata	2000	8.05	0.24

In order to fully understand the distribution of in situ stress in coal seams and comprehensively analyze the influence of normal fault on in situ stress, as shown in Figure 5, two measuring lines were arranged along the x-direction on the horizontal plane located in the middle of the hanging wall and footwall coal seams to monitor the changes in geostress at different positions. The burial depths of the two horizontal planes were 3237 m and 3227 m, respectively. At the same time, two measuring points, P_1 and P_2, were arranged at the intersection of measuring line 1 and the fault boundary.

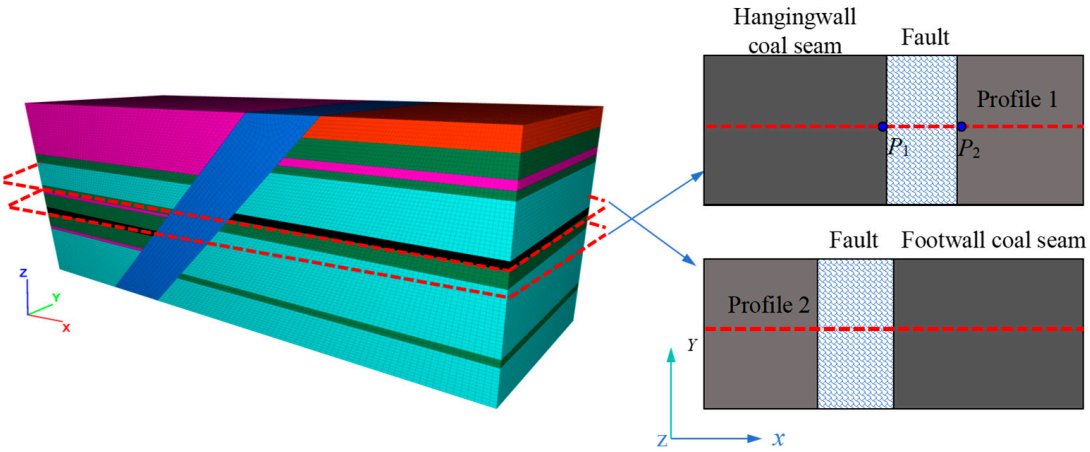


Figure 5. The layout of stress measurement lines and points in the middle of the coal seam.

Considering the numerous factors that affect coal seam stress, based on the previous model, seven parameters including coal's elastic modulus, coal's Poisson's ratio, the coal seam thickness, fault elastic modulus, fault Poisson's ratio, fault thickness, and fault dip were selected for a sensitivity analysis of coal seam stress changes. The specific parameter values are shown in Table 2, with three values selected for each factor. The values in the basic model were reduced by 20% as the lower value and increased by 20% as the upper value.

Table 2. Parameter sensitivity analysis scheme table.

Parameters		Lower Value	Based Value	Upper Value
Coal seam	**Elastic modulus E_c/GPa**	2.984	3.73	4.476
	Poisson's ratio v_c	0.28	0.35	0.42
	Thickness/m	1	2	3
Fault	**Elastic modulus E_f/GPa**	6.44	8.05	9.66
	Poisson's ratio v_f	0.192	0.24	0.288
	Thickness/m	16	20	24
	Dip/°	36	45	54

4. Simulation Results

4.1. The Distribution of In Situ Stress in the Hanging Wall Coal Seam

Figure 6 displays the three principal stress contour maps of the transverse plane in the middle of the overlying coal seam in the model, along with the stress curve at measurement line 1. It is evident that the fault significantly affects the uneven stress distribution, primarily causing a notable weakening of stress in the fault zone compared to other areas. The stress at the end of the fault is close to the original stress, and the stress concentration phenomenon in the footwall strata near the fault is obvious. The far-field strata in the footwall strata maintain the original stress size and are less affected by the fault. The phenomenon of stress weakening occurs in the hanging wall coal seam, and the closer it is to the fault, the more obvious the stress weakening phenomenon becomes. The three principal stress variation curves at measurement line 1 all exhibit obvious V-shaped characteristics, with the magnitude of the three principal stresses decreasing first. When the stress decreases to the vicinity of the fault, the curve fluctuates, and then rapidly rises and gradually stabilizes. The maximum horizontal stress undergoes significant fault-induced variation, exhibiting large differences between the hanging wall and footwall strata. In contrast, vertical stress differences across the fault are relatively minor. The main reason for the stress distribution characteristics mentioned above is that both the overlying coal seam

and the fault are weak strata, which undergo significant deformation under external forces, leading to stress release and transfer. In contrast, the rock in the lower strata has a higher elastic modulus and stronger resistance to deformation, especially when subjected to more stress near the fault, resulting in stress concentration. The far-field strata are less affected by the fault and maintain their original stress level.

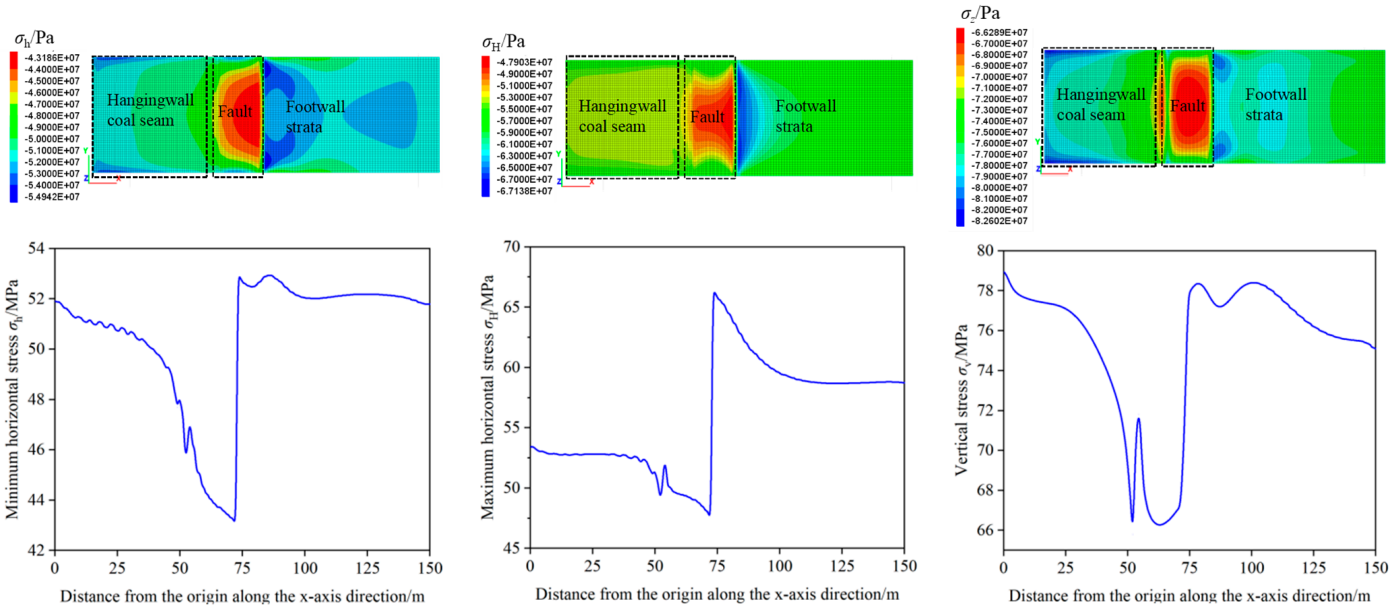


Figure 6. Cloud maps of in situ stress distribution in the plane where the coal seam is located on the hanging wall and the in situ stress curves at measurement line 1.

4.2. The Distribution of In Situ Stress in the Footwall Coal Seam

Figure 7 presents the three principal stress contour maps of the transverse plane at the middle of the lower coal seam in the basic model along with stress curves at measurement line 2. The stress distribution in this plane exhibits strong non-uniformity. Stress weakening is evident at the fault, with stress concentration occurring in the overlying strata nearby. Far-field stress remains close to the initial in situ stress and is minimally affected by the fault. From the stress variation curve at measuring line 2, it can be seen that similarly to the plane where the hanging coal seam is located, the curve trend still presents a typical V shape. However, contrary to the hanging coal seam, at the same depth, the stress in the strata on the left side of the fault is higher than that in the coal seam on the right side of the fault. Among them, the stress difference on both sides of the fault is the most obvious in the maximum horizontal stress, indicating that the maximum horizontal stress in the lower coal seam is greatly affected by the coal seam and has a higher degree of weakening. The main reason for this is that the burial depth of the lower strata is relatively large. Under the action of large vertical stress, significant deformation occurs along the direction of the maximum horizontal stress, which counteracts the maximum horizontal stress. Under the Poisson effect, the maximum horizontal stress decreases, and it decreases more than the minimum horizontal stress.

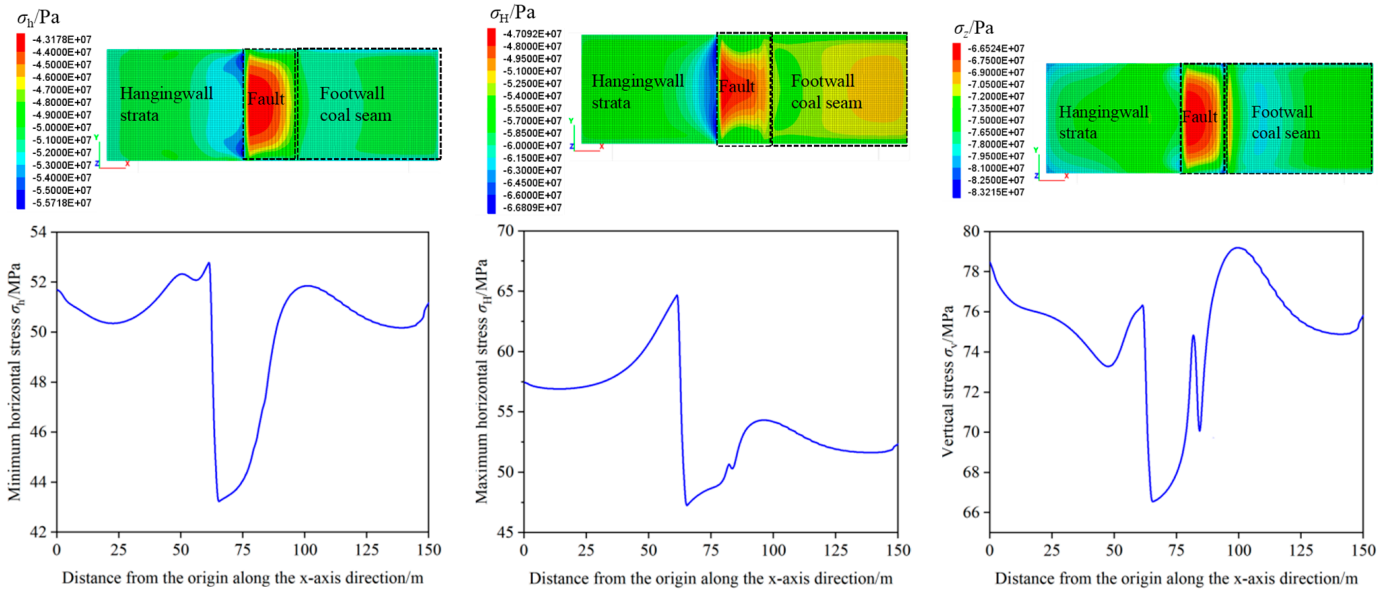


Figure 7. Cloud maps of in situ stress distribution on the plane where the footwall coal seam is located and stress curves at measurement line 2.

4.3. Parameter Sensitivity Analysis

From the analysis of the distribution characteristics of in situ stress in the basic model in the previous text, it can be seen that there are significant changes in the two horizontal in situ stresses in the coal seam, while the vertical in situ stress is mainly affected by gravity, which only changes at the local position where the fault intersects with the coal seam. Therefore, based on the basic model, we focus on analyzing the changes in horizontal in situ stress in the coal seams under the influence of different parameters.

(1) Coal elastic modulus

Figure 8 shows the horizontal stress variation curves at the measured line in the middle of the hanging wall and footwall coal seams under different coal rock elastic modulus conditions. It can be seen from the figure that regardless of whether it is the hanging wall or footwall coal seam, the variation in the coal rock elastic modulus has a greater impact on the stress in the coal seam, followed by the impact on the fault, and it has a smaller impact on the other strata at the same horizontal plane of the coal seam, with only some changes occurring near the fault. The horizontal stress in coal seams is positively correlated with the elastic modulus of coal rock, while the stress in faults is negatively correlated with the elastic modulus of coal rock. At the same time, when the elastic modulus changes by the same value, the minimum horizontal stress changes more than the maximum horizontal stress. The primary factor is that an increase in coal rock's elastic modulus enhances its deformation resistance, reducing deformation and stress transfer, and consequently decreasing weakening.

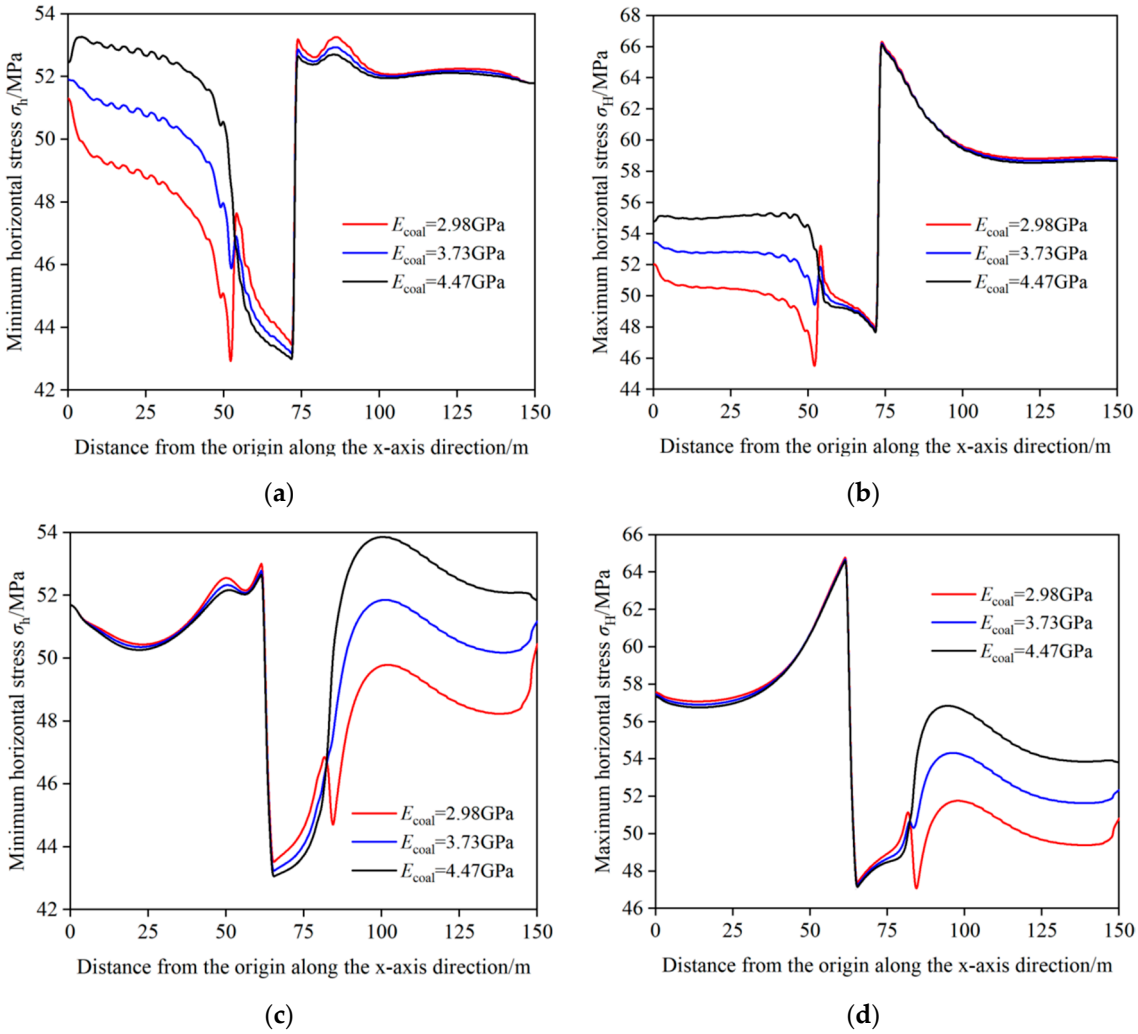


Figure 8. The stress variation curves at the measuring line under different coal elastic modulus values: (**a**) σ_h at measuring line 1; (**b**) σ_H at measuring line 1; (**c**) σ_h at measuring line 2; (**d**) σ_H at measuring line 2.

(2) Poisson's ratio of coal seam

Figure 9 shows the horizontal stress variation curves at the middle measuring line of the hanging wall and footwall coal seams under different Poisson's ratios for coal rock. It can be seen from the figure that compared to the elastic modulus of coal rock, the change in the Poisson's ratio has a greater impact on the horizontal stress in the strata, especially for coal seams. The horizontal stress in the coal seam is positively correlated with the Poisson's ratio. When the Poisson's ratio is 0.42, the overall horizontal stress in the coal seam increases and is higher than that in other strata at the same level. Compared with the stress in the coal seam, the fault and other strata are less affected by the Poisson's ratio, and their horizontal stress is negatively correlated with the Poisson's ratio. The main reason for the above phenomenon is that when the Poisson's ratio is high, the coal seam undergoes significant lateral deformation under external forces, especially gravity, and the vertical stress increases, resulting in an increase in horizontal stress and affecting the overall stress distribution of the coal seam.

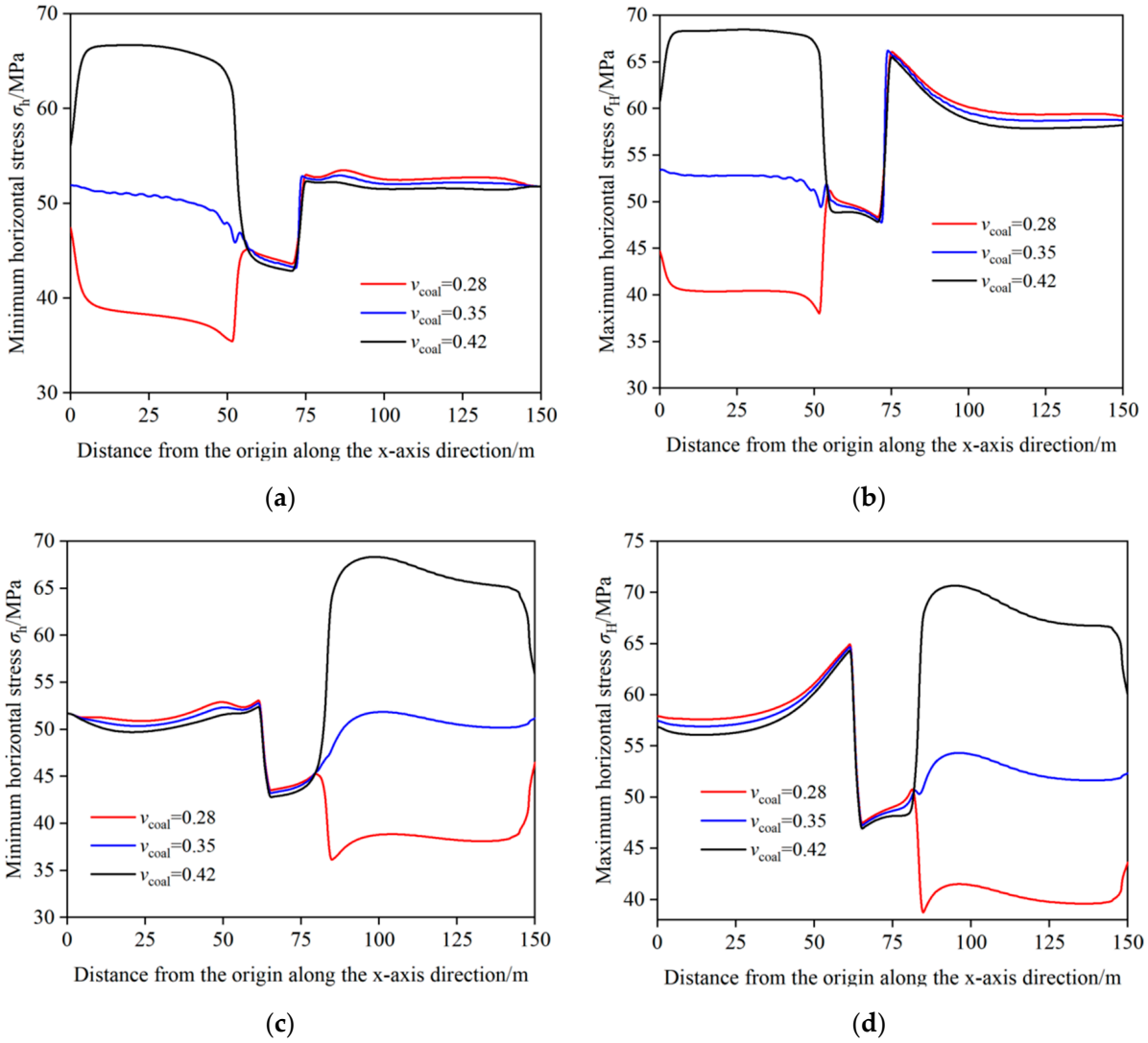


Figure 9. Stress variation curves at measurement lines under different Poisson's ratios for coal rock: (**a**) σ_h at measuring line 1; (**b**) σ_H at measuring line 1; (**c**) σ_h at measuring line 2; (**d**) σ_H at measuring line 2.

(3) Coal seam thickness

Figure 10 shows the horizontal stress variation curves at the measuring line in the middle of the hanging wall and footwall coal seams when the coal seam thickness is 1.6 m, 2.0 m, and 2.4 m, respectively. It can be seen from the figure that the coal seam thickness has a small impact on horizontal stress. Under different working conditions, the overall trend of the stress curve at the measuring line is consistent, and the values are similar. The main reason for this is that the coal seam studied in this article comprises thin coal layers. When the coal seam thickness changes, it only has a certain impact on the self-weight of the formation, resulting in a slight change, and thus, the impact on the horizontal stress is also small.

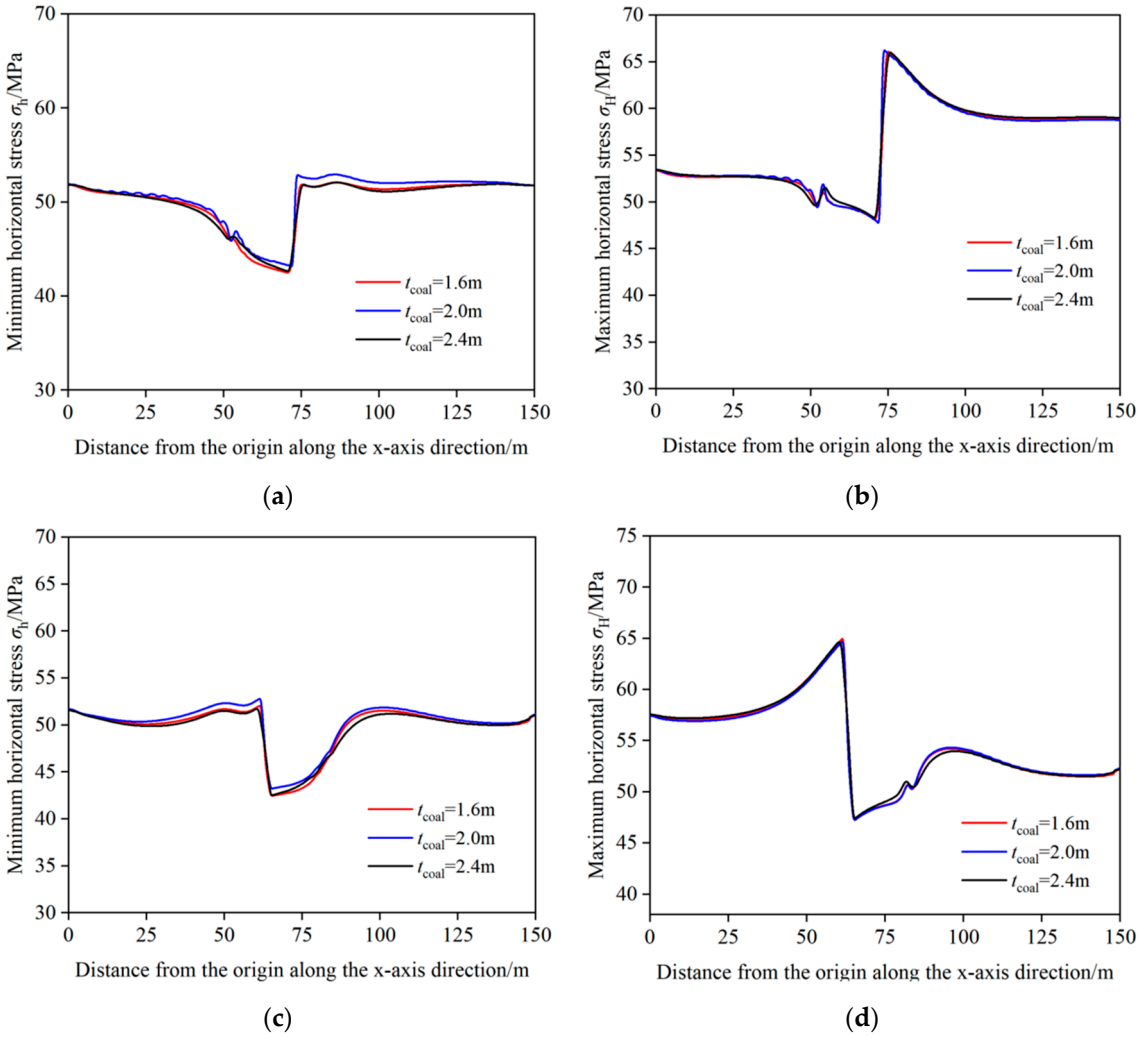


Figure 10. Stress variation curves at measurement lines under different coal seam thickness conditions: (**a**) σ_h at measuring line 1; (**b**) σ_H at measuring line 1; (**c**) σ_h at measuring line 2; (**d**) σ_H at measuring line 2.

(4) Fault elastic modulus

Figure 11 shows the influence of different fault elastic modulus values on the horizontal stress at the measurement line. Overall, the horizontal stresses of both the hanging wall and footwall strata are influenced by the fault's elastic modulus, with the most significant effect occurring within the fault itself, followed by areas near the fault. The far-field strata far away from the fault remain almost unchanged, and the maximum horizontal stress is more affected by the elastic modulus of the fault than the minimum horizontal stress. The stress inside the fault is positively correlated with the elastic modulus of the fault rock, while the coal seams and other rock layers on both sides of the fault are inversely proportional to the elastic modulus of the fault. The main reason for the above phenomenon is that when the elastic modulus of the rock inside the fault increases, its ability to resist external forces and withstand deformation increases. Under the same external force conditions, the deformation amount is smaller, and the transfer of stress to the relatively hard rocks on both sides decreases. As a result, fault internal stress rises, while stress in surrounding rock masses decreases accordingly as the fault rock bears more of the external load.

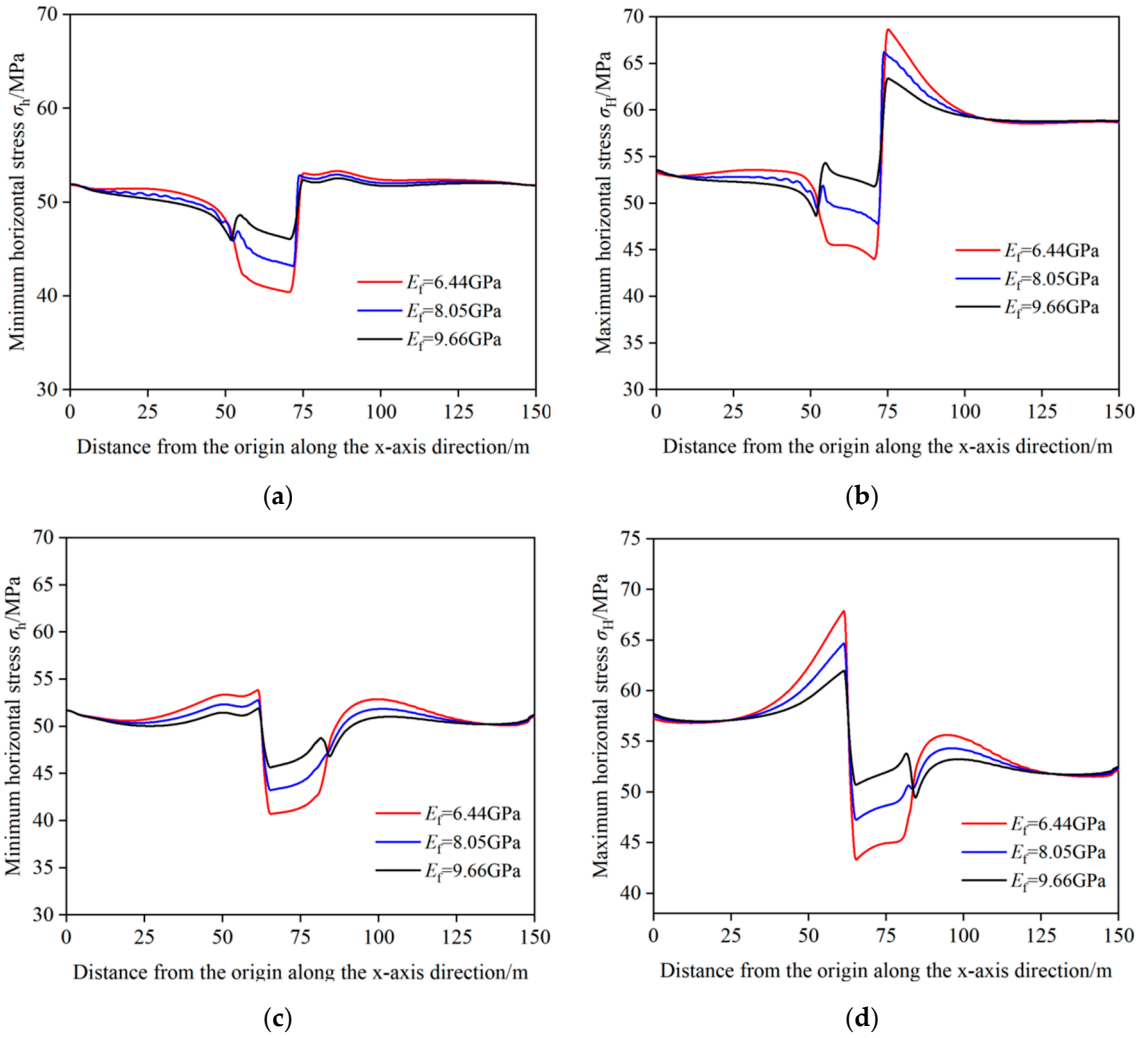


Figure 11. Stress variation curves at measurement lines under different elastic modulus conditions of fault rocks: (**a**) σ_h at measuring line 1; (**b**) σ_H at measuring line 1; (**c**) σ_h at measuring line 2; (**d**) σ_H at measuring line 2.

(5) Poisson's ratio of fault

Figure 12 shows the variation in the Poisson's ratio on the horizontal stress of rocks in different fault fracture zones. The figure highlights that the strata most influenced by fault Poisson's ratios are located within and adjacent to the fault. The stress within the fault is positively correlated with the Poisson's ratio, while the stress on both sides of the strata is negatively correlated with the Poisson's ratio of the fault. Among them, the stress in the hanging coal seam is less affected by the Poisson's ratio of the fault, and the difference between the curves of different Poisson's ratios is small. In the hanging wall and footwall strata, whether there are coal seams or other strata, the maximum horizontal stress is more influenced by the Poisson's ratio than the minimum horizontal stress. The primary cause of this phenomenon is increased fault Poisson's ratios, which subject fault rocks to external forces, notably the gravity of overlying layers, causing significant lateral deformation. Due to the limitations of horizontal external forces on both sides, the vertical stress increases, which also leads to an increase in horizontal stress. When the external force on the rocks inside the fault increases, the transfer of stress to the rock layers on both sides decreases, resulting in a decrease in horizontal stress inside the rocks on both sides.

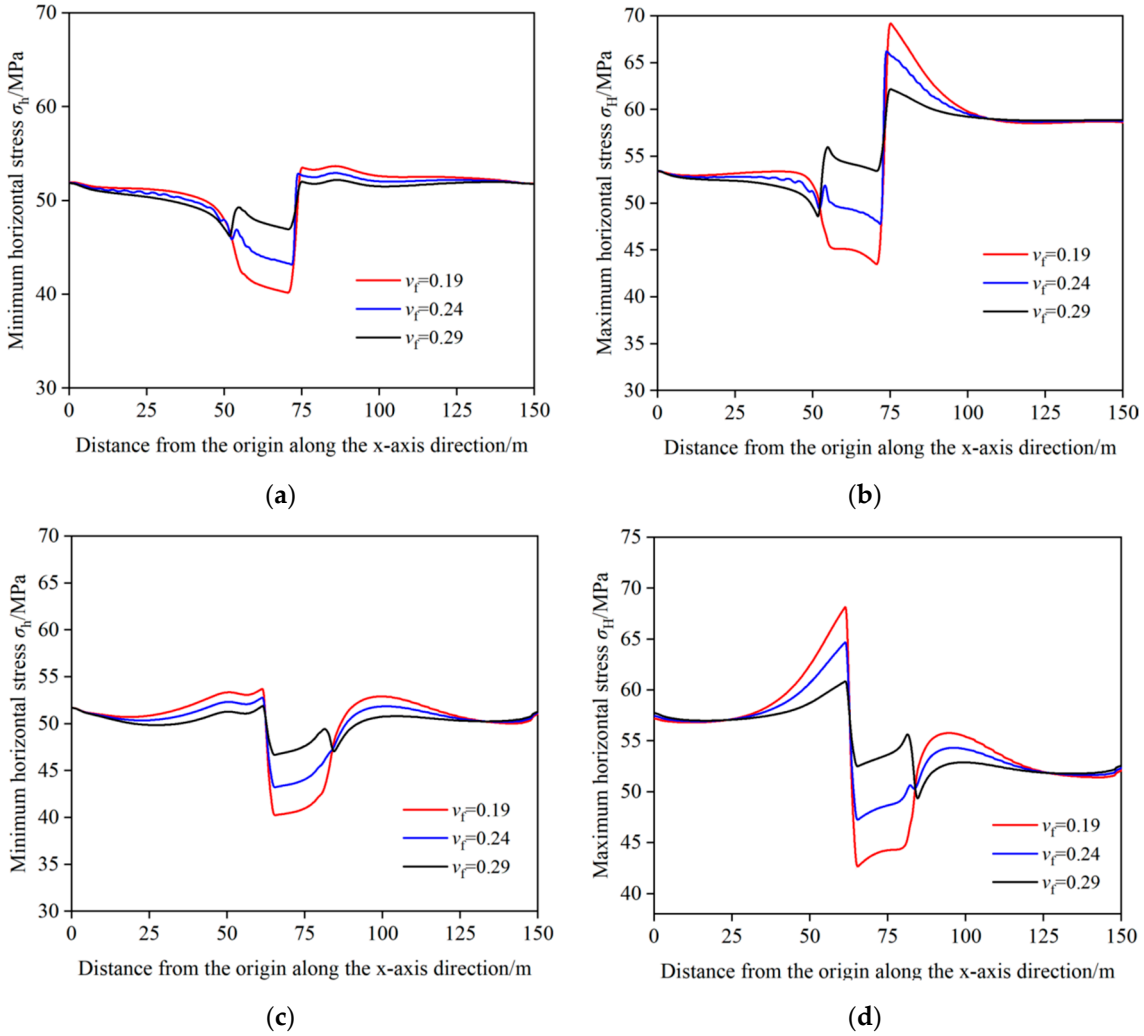


Figure 12. Stress variation curves at measurement lines under different Poisson's ratios for fault rocks: (**a**) σ_h at measuring line 1; (**b**) σ_H at measuring line 1; (**c**) σ_h at measuring line 2; (**d**) σ_H at measuring line 2.

(6) Fault thickness

Figure 13 shows the variation law of horizontal stress in the strata at the measuring line under different fault thicknesses. The figure clearly shows that fault thickness has a lesser impact on stress in strata compared to rock properties like the elastic modulus and Poisson's ratio. The main difference in stress values is due to the different stress influence ranges of fault thickness. The stress values in the hanging coal seams of different thicknesses are almost unaffected by the fault thickness, with only slight fluctuations near the fault. At this time, the stress curves inside the fault almost overlap. The maximum horizontal in situ stress is more affected by the thickness of the fault than the minimum horizontal in situ stress, especially in the fault and other strata, except for coal seams. The maximum horizontal in situ stress within the fault is positively correlated with the thickness, and the geological stress at the stress concentration point is also positively correlated with the thickness. This is primarily due to geometric effects. Thicker faults cause greater deformation in a wider range of strata, and an increased fault thickness leads to higher gravity loads on adjacent rock layers, especially those with a high elastic modulus, enhancing the stress concentration.

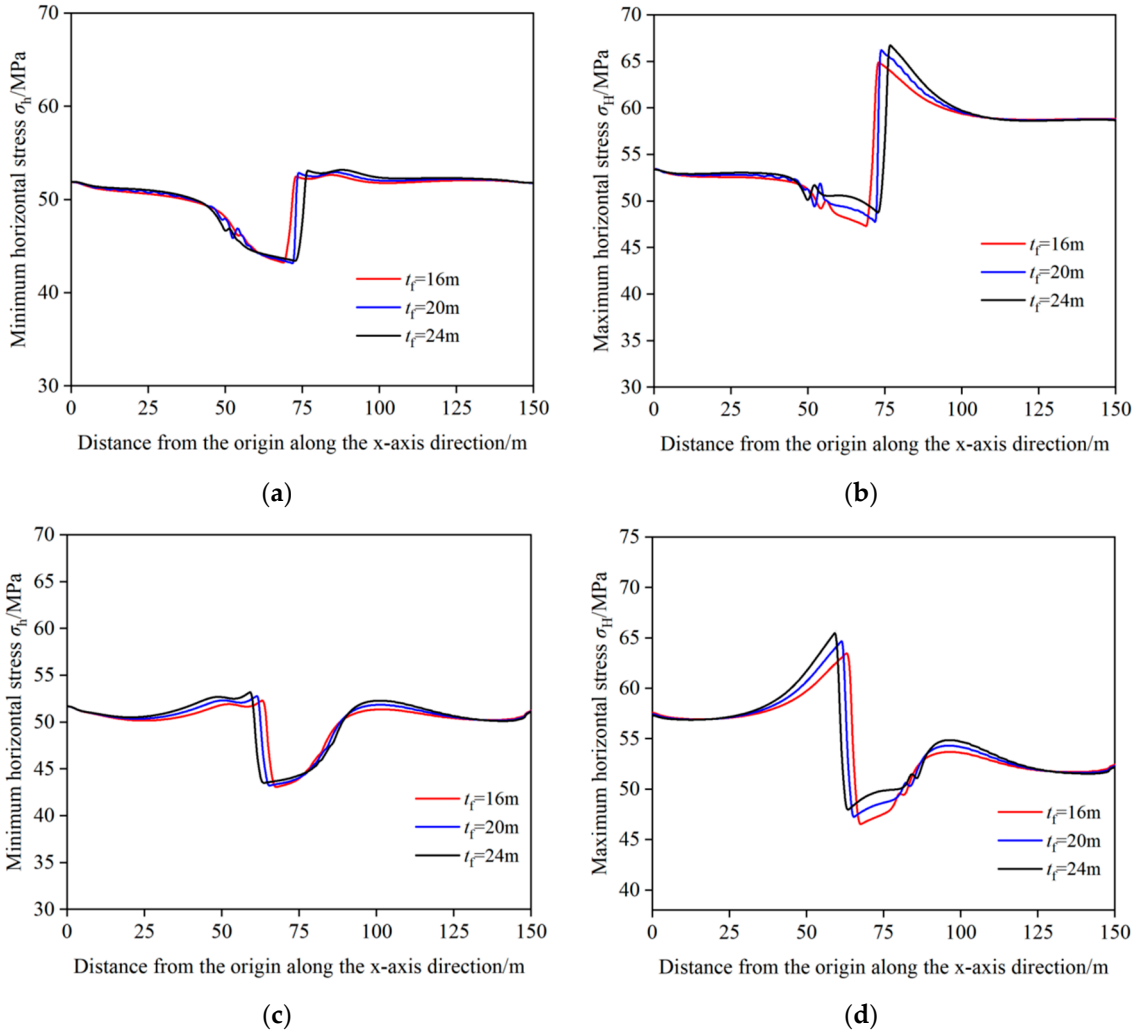


Figure 13. Stress variation curves at measurement lines under different fault thickness conditions: (**a**) σ_h at measuring line 1; (**b**) σ_H at measuring line 1; (**c**) σ_h at measuring line 2; (**d**) σ_H at measuring line 2.

(7) Fault dip angle

Figure 14 depicts the variation in horizontal in situ stress at the measuring line influenced by different fault dip angles. The figure reveals slight variations in strata impact based on fault location and dip angle. Both the hanging wall and footwall strata, particularly at the fault and coal seam areas, are notably affected by the fault dip angle. The minimum horizontal in situ stress in other strata at the same level as the coal seam is minimally affected by the fault dip angle, and the maximum horizontal in situ stress only changes slightly near the fault. The stress concentration is more obvious in the case of a large fault dip angle. In the fault and coal seam areas near the fault, the horizontal stress is directly proportional to the dip angle of the fault. The main reason for this is still related to the structure of the fault. When the dip angle of the fault is smaller and closer to the horizontal plane, the fault plane will bear more weight from the overlying rock layers. Therefore, the fault plane will undergo more normal deformation, and the trend of shear slip will decrease, leading to further reductions in overall deformation and horizontal stress.

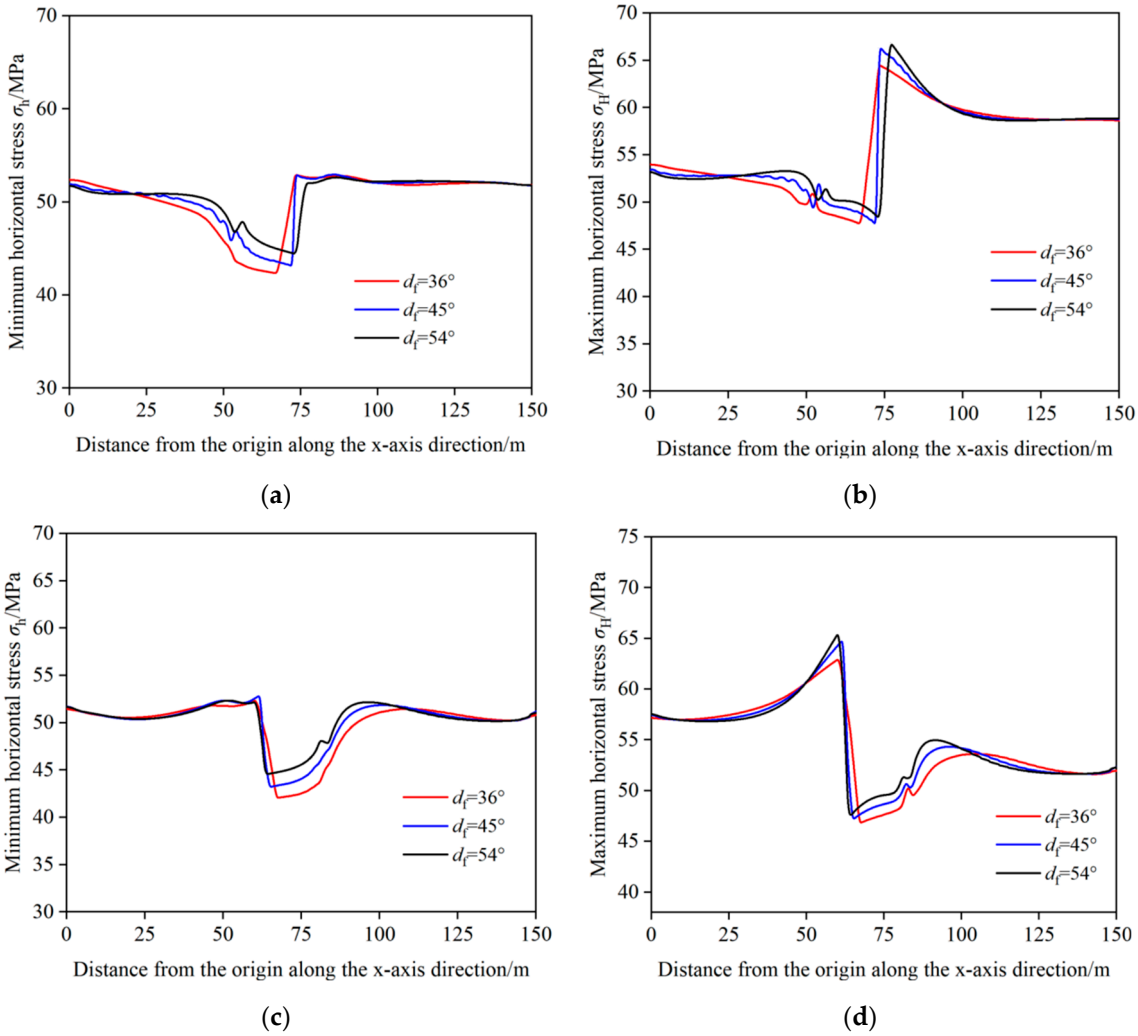


Figure 14. Stress variation curves at measurement lines under different fault dip angles: (**a**) σ_h at measuring line 1; (**b**) σ_H at measuring line 1; (**c**) σ_h at measuring line 2; (**d**) σ_H at measuring line 2.

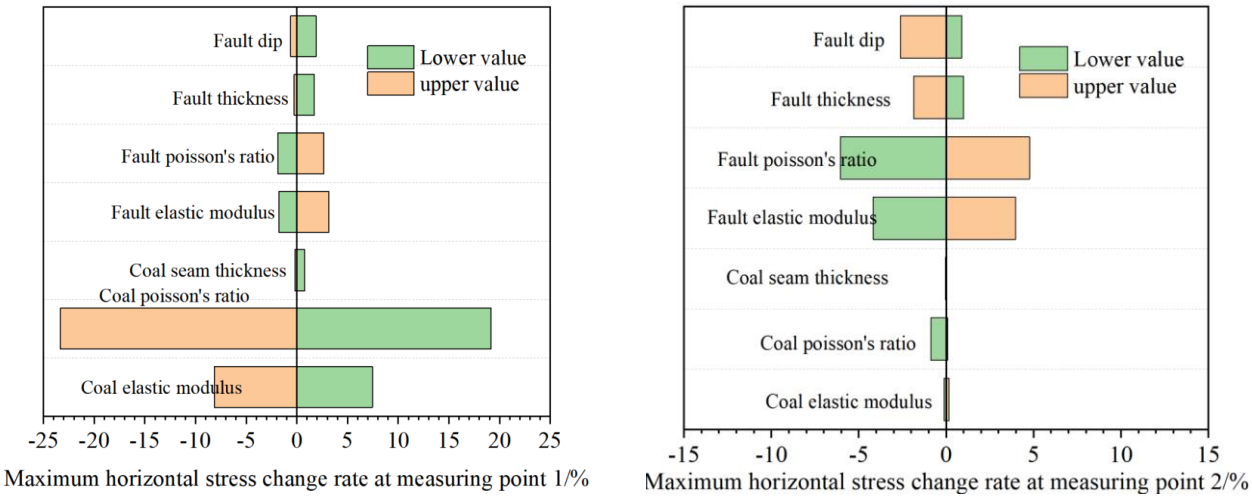
(8) Influence weight analysis

From previous research, it can be found that the existence of faults has similar effects on the hanging wall and footwall coal seams, that is, both will cause the weakening of stress in the coal seam near the fault, resulting in stress concentration on the other side. This change mainly occurs in the discontinuous area near the fault. In addition, the maximum horizontal stress is more affected by the fault than the minimum horizontal stress, and the influence of different fault and coal seam parameters on the stress also varies. In order to further analyze the influence weight of different parameters on the stress, by taking the maximum horizontal stress at the boundary of the plane rock layer where the hanging wall coal seam is located as an example, the maximum horizontal stress was statistically analyzed at different measuring points under different working conditions, and the change rate of stress was calculated when the parameter value changed. The specific results are shown in Table 3.

Table 3. Statistical table of maximum horizontal in situ stress at measuring points under different parameter conditions.

Parameters	Measuring Point 1				Measuring Point 2			
	Lower Value/MPa	Change Rate/%	Upper Value/MPa	Change Rate/%	Lower Value/MPa	Change Rate/%	Upper Value/MPa	Change Rate/%
Elastic modulus of coal	45.13	−8.16%	52.80	7.45%	66.36	0.15%	66.17	−0.14%
Poisson's ratio of coal	37.68	−23.32%	65.56	19.17%	66.31	0.08%	65.67	−0.89%
Coal seam thickness	49.04	−0.20%	49.52	0.77%	66.22	−0.06%	66.12	0.03%
Fault elastic modulus	50.69	3.15%	48.27	−1.77%	68.88	3.95%	63.49	−4.18%
Poisson's ratio of fault	50.44	2.65%	48.22	−1.87%	69.41	4.75%	62.24	−6.07%
Fault thickness	49.71	−0.26%	49.98	1.71%	65.02	−1.87%	66.91	0.98%
Fault dip	49.74	−0.61%	50.07	1.89%	64.52	−2.63%	66.84	0.88%

As shown in Figure 15, the rate of change in geostress is plotted as a bar chart for analysis. From bar Figure 15a, it can be observed that the coal's Poisson's ratio, the coal's elastic modulus, and the fault dip angle are negatively correlated with the horizontal stress in the coal seam, while the other parameters are positively correlated with the horizontal stress in the coal seam. The degree of influence of the rate of change on the weakening of the geostress in the coal seam can be summarized as follows: Poisson's ratio > elastic modulus > fault elastic modulus > fault Poisson's ratio > fault dip angle > fault thickness > coal seam thickness. When the Poisson's ratio of coal rock decreases by 20%, the maximum horizontal geostress at measuring point 1 actually decreases by 23.32%. From Figure 15b, it can be seen that the influence of various parameters on the lower strata is lower than that on the upper strata, and the stress in the lower strata is almost unaffected by the upper coal seam. The influence of fault parameters on the lower strata dominates, and the degree of influence can be ranked as fault Poisson's ratio > fault elastic modulus > fault dip angle > fault thickness. When the Poisson's ratio of the rock in the fault layer increases by 20%, the maximum horizontal stress at measuring point 2 decreases by 6.07%, while when the coal seam thickness increases by 20%, the maximum horizontal stress at measuring point 2 only decreases by −0.06% with little impact.



(**a**) Measuring point 1 (**b**) Measuring point 2

Figure 15. Bar chart of maximum horizontal in situ stress change rate at different measuring points.

5. Conclusions

This article focuses on the complex and diverse distribution of coal seam stress under the influence of normal fault. Taking the LF M1 oilfield as the research background, a

3D strata numerical model containing normal fault was established using FLAC3D. The distribution law of in situ stress considering the influence of normal fault was systematically studied. The main conclusions are as follows:

1. The existence of normal fault makes the in situ stress in the transverse plane where the coal seam is located produce obvious non-uniform and discontinuous characteristics. In the stratum near the fault, the in situ stress in the coal seam produces an obvious weakening phenomenon, a strong stress concentration phenomenon occurs on both sides of the fault, and the in situ stress in the far field area far away from the fault is close to the original stress without obvious change.
2. There are significant differences in the influence of different parameters on in situ stress. The Poisson's ratio of coal, the elastic modulus of coal, and the fault dip are negatively correlated with the horizontal stress in the coal seam, while other parameters are positively correlated with the horizontal stress in the coal seam. The maximum horizontal stress is more affected by parameter changes than the minimum horizontal stress.
3. According to the change rate of in situ stress, the degree of influence of various factors on the weakening of coal seam in situ stress can be ranked as follows: coal's Poisson's ratio > coal's elastic modulus > fault elastic modulus > fault's Poisson's ratio > fault dip angle > fault thickness > coal seam thickness. And the coal seam parameters have almost no effect on the stress on the other side of the fault. In short, the stress distribution near the fault is complex due to the joint influence of fault occurrence, rock mechanics parameters, and external loads. This area is a potential area for drilling accidents, such as wellbore instability, leakage, and reservoir damage, and this should be carefully considered during drilling.
4. It is worth noting that this study only provides a preliminary understanding of the distribution law of coal seam stress under the influence of normal faults. In the future, further research will be carried out around the following aspects: establishing complex geometric models while considering the distribution law of elastic–plastic geological stress under the influence of multiple faults and inclined coal seams; establishing a 3D loading experimental system for geological strata, and conducting indoor physical simulation experiments of similar materials and comparing them with numerical simulations; and conducting numerical simulations of geostress that comprehensively consider fluid structure coupling effects, geological anisotropy, and heterogeneity.

Author Contributions: Methodology, Z.R. and Y.L.; Software, Y.L.; Validation, Q.D.; Formal Analysis, Q.D.; Investigation, C.X. and Z.H.; Resources, Z.R.; Data Curation, Q.D. and C.X.; Writing—Original Draft, Y.L.; Writing—Review and Editing, Y.L.; Visualization, C.X.; Supervision, Z.H.; Project Administration, Z.R. and Z.H.; Funding Acquisition, Z.H. All authors have read and agreed to the published version of the manuscript.

Funding: This research received no external funding.

Data Availability Statement: The data are contained within the article.

Conflicts of Interest: Authors Zhihua Rao, Qingjie Du and Chunsheng Xiang were employed by the company CNOOC China Ltd. The remaining authors declare that the research was conducted in the absence of any commercial or financial relationships that could be construed as a potential conflict of interest.

References

1. Pidho, J.J.; Liang, Y.B.; Cheng, Y.F.; Yan, C.L. Analysis of interaction of hydraulic fractures with natural fractures and bedding planes in layered formation through cohesive zone modelling. *Theor. Appl. Fract. Mech.* **2023**, *123*, 103708. [CrossRef]
2. Liang, Y.B.; Cheng, Y.F.; Han, Z.Y.; Yan, C.L. Numerical Simulation Analysis on Production Evolution Laws in Shale Reservoirs Considering a Horizontal Well Interwell Interference Effect. *Energy Fuels* **2024**, *38*, 4076–4090. [CrossRef]
3. Jiang, N.; Wang, C.X.; Pan, H.Y.; Yin, D.W.; Ma, J.B. Modeling study on the influence of the strip filling mining sequence on mining-induced failure. *Energy Sci. Eng.* **2020**, *8*, 2239–2255. [CrossRef]
4. Lu, X.Z.; Xu, Y.J.; Tian, Y.; Cetiner, B.; Taciroglu, E. A deep learning approach to rapid regional post-event seismic damage assessment using time-frequency distributions of ground motions. *Earthq. Eng. Struct. Dyn.* **2021**, *50*, 1612–1627. [CrossRef]
5. Lu, W.; Meng, L.X.; Li, S.C.; Xu, Y.D.; Wang, L.; Zhang, P.; Dou, S.; Sun, H.B. Study on progressive failure behavior and mechanical properties of tunnel arch support structures. *Tunn. Undergr. Space Technol.* **2023**, *140*, 105285. [CrossRef]
6. Zhu, C.; He, M.C.; Karakus, M.; Zhang, X.H.; Tao, Z.G. Numerical simulations of the failure process of anaclinal slope physical model and control mechanism of negative Poisson's ratio cable. *Bull. Eng. Geol. Environ.* **2021**, *80*, 3365–3380. [CrossRef]
7. Zhou, Q.L.; Liu, D.P.; Lin, X.D. Pre-evaluation of fault stability for underground mining based on geomechanical fault-slip analysis. *Geomat. Nat. Hazards Risk* **2022**, *13*, 400–413. [CrossRef]
8. Zhang, S.Y.; Shi, L.; Jia, D.L. An uncertainty quantitative model of wellbore failure risk for underground gas storage in depleted gas reservoir during the construction process. *J. Energy Storage* **2023**, *57*, 106144. [CrossRef]
9. Zhang, K.H.; Zhou, Y.S.; Liu, Y.M.; Wang, P. Mechanism for seismic supershear dynamic rupture based on in-situ stress: A case study of the Palu earthquake in 2018. *Geomat. Nat. Hazards Risk* **2022**, *13*, 1987–2005. [CrossRef]
10. Kruszewski, M.; Montegrossi, G.; Balcewicz, M.; Igbokwe, O.A.; Backers, T.; Saenger, E.H. 3D in situ stress state modelling and fault reactivation risk exemplified in the Ruhr region (Germany). *Geomech. Energy Environ.* **2022**, *32*, 100386. [CrossRef]
11. Guo, W.H.; Cao, A.Y.; Hu, Y.; Xue, C.C.; Liu, Y.Q.; Lv, D.Z. Stress distribution and rockburst characteristics of roadway group under the influence of fault and fold structures: A case study. *Geomat. Nat. Hazards Risk* **2022**, *13*, 736–761. [CrossRef]
12. Liu, Y.; Liu, S.L.; Huo, Z.C.; Sun, K.; Wang, T.; Li, W.G. Failure Characteristics of Coal Seam Floor and Risk Assessment of Water Inrush Caused by Underground Coal Mining. *Energy Explor. Exploit.* **2023**, *41*, 677–695. [CrossRef]
13. Li, P.; Ren, F.H.; Cai, M.F.; Guo, Q.F.; Miao, S.J. Present-day stress state and fault stability analysis in the capital area of China constrained by in situ stress measurements and focal mechanism solutions. *J. Asian Earth Sci.* **2019**, *185*, 104007. [CrossRef]
14. Li, P.; Cai, M.F.; Guo, Q.F.; Ren, F.H.; Miao, S.J. Current stress field and its relationship to tectonism in a coal mining district, central China, for underground coal energy exploration. *Energy Rep.* **2022**, *8*, 5313–5328. [CrossRef]
15. Li, P.; Cai, M.F.; Miao, S.J.; Guo, Q.F. New Insights into the Current Stress Field Around the Yishu Fault Zone, Eastern China. *Rock Mech. Rock Eng.* **2019**, *52*, 4133–4145. [CrossRef]
16. Yuan, D.; Zhang, L.B.; Liu, X.L.; Feng, T.; Zhang, G.Z.; Xu, Z.X.; Wang, Z.; Yi, X.; Lin, Z.; Ren, L.; et al. Influence of the Xianshuihe Fault Zone on In-Situ Stress Field of a Deep Tunnel and its Engineering Effect. *Front. Earth Sci.* **2022**, *10*, 886876. [CrossRef]
17. Ji, M.; Guo, H.J. Influence of in-situ rock stress on the stability of roadway surrounding rock: A case study. *J. Geophys. Eng.* **2020**, *17*, 138–147. [CrossRef]
18. Cheng, X.G.; Qiao, W.; Dou, L.M.; He, H.; Ju, W.; Zhang, J.K.; Song, S.; Cui, H.; Fang, H.Z. In-situ stress field inversion and its impact on mining-induced seismicity. *Geomat. Nat. Hazards Risk* **2023**, *14*, 176–195. [CrossRef]
19. Yong, R.; Wu, J.F.; Huang, H.Y.; Xu, E.R.; Xu, B. Complex in situ stress states in a deep shale gas reservoir in the southern Sichuan Basin, China: From field stress measurements to in situ stress modeling. *Mar. Pet. Geol.* **2022**, *141*, 105702. [CrossRef]
20. Zhao, X.G.; Wang, J.; Qin, X.H.; Cai, M.; Su, R.; He, J.G.; Zong, Z.; Ma, L.; Ji, R.; Zhang, M.; et al. In-situ stress measurements and regional stress field assessment in the Xinjiang candidate area for China's HLW disposal. *Eng. Geol.* **2015**, *197*, 42–56. [CrossRef]
21. Roshan, H.; Li, D.Q.; Canbulat, I.; Regenauer-Lieb, K. Borehole deformation based in situ stress estimation using televiewer data. *J. Rock Mech. Geotech. Eng.* **2023**, *15*, 2475–2481. [CrossRef]
22. Jiang, L.S.; Wang, P.; Zheng, P.Q.; Luan, H.J.; Zhang, C. Influence of Different Advancing Directions on Mining Effect Caused by a Fault. *Adv. Civ. Eng.* **2019**, *2019*, 7306850. [CrossRef]
23. Wang, P.; Jiang, L.S.; Zheng, P.Q. Application of equivalent materials to modeling fractures in the vicinity of a normal fault in the area of mining exploitation influence. *Acta Geodyn. Geomater.* **2017**, *14*, 475–485. [CrossRef]
24. Wang, P.; Jiang, L.S.; Li, X.Y.; Qin, G.P.; Wang, E.Y. Physical simulation of mining effect caused by a fault tectonic. *Arab. J. Geosci.* **2018**, *11*, 741. [CrossRef]
25. Su, Z.D.; Zhou, S.Z.; Zang, A.N.; Sun, J.Z.; Zhang, T.; Niu, Y.; Zhang, J.; Liang, J. Correction to: Analysis of Near-Field Stresses in an Analogue Strike-Slip Fault Model. *Rock Mech. Rock Eng.* **2024**, *57*, 4129. [CrossRef]
26. Lin, P.; Liu, H.Y.; Zhou, W.Y. Experimental study on failure behaviour of deep tunnels under high in-situ stresses. *Tunn. Undergr. Space Technol.* **2015**, *46*, 28–45. [CrossRef]
27. Hao, X.J.; Yuan, L.; Xue, J.H.; Wang, S.H.; Ren, B.; Zhang, X.Y.; Li, Y.L. Physical Model Test and Evaluation for the Tunnel Stability Influenced by Magnitude and Path of Loading. *J. Test. Eval.* **2020**, *48*, 1452–1477. [CrossRef]

28. Feng, X.T.; Li, Z.W.; Mei, S.M.; Tian, J.; Yang, C.X.; Yao, Z.B.; Gao, J.K. A Novel Large-Scale Three-Dimensional Physical Model Experimental System for Deep Underground Engineering. *Rock Mech. Rock Eng.* **2023**, *56*, 8395–8413. [CrossRef]
29. Ju, Y.; Wan, C.B.; Fu, G.M.; Ren, Z.Y.; Mao, L.T.; Chiang, F.P. Effects of near-fault stress evolution and surface asperities on rough fault slip: An evaluation based on photoelastic shear tests and additively printed models. *Eng. Geol.* **2022**, *305*, 106715. [CrossRef]
30. Giorgetti, C.; Tesei, T.; Scuderi, M.M.; Collettini, C. Experimental Insights Into Fault Reactivation in Gouge-Filled Fault Zones. *J. Geophys. Res. Solid Earth* **2019**, *124*, 4189–4204. [CrossRef]
31. Yin, S.; Xie, R.C.; Wu, Z.H.; Liu, J.; Ding, W.L. In situ stress heterogeneity in a highly developed strike-slip fault zone and its effect on the distribution of tight gases: A 3D finite element simulation study. *Mar. Pet. Geol.* **2019**, *99*, 75–91. [CrossRef]
32. Karatela, E.; Taheri, A. Localized stress field modelling around fractures using three-dimensional discrete element method. *J. Pet. Sci. Eng.* **2018**, *171*, 472–483. [CrossRef]
33. Jiang, L.S.; Wang, P.; Zhang, P.P.; Zheng, P.Q.; Xu, B. Numerical analysis of the effects induced by normal faults and dip angles on rock bursts. *C. R. Mec.* **2017**, *345*, 690–705. [CrossRef]
34. Ai, K.; Zhang, X.H.; Zhou, C. Study on the Method for Measuring Stress on Rock Mass Excavation Surface under Extremely High Stress Conditions. *Geofluids* **2022**, *2022*, 4509192. [CrossRef]
35. Xu, D.Y.; Si, H.; Hu, Q.T.; Liang, Y.P. Quantitative Study on the Stress Distribution Characteristics of Coal Rock with Faults. *Geofluids* **2022**, *2022*, 8214322. [CrossRef]
36. Xu, D.Y.; Hu, Q.T.; Si, H. Measurement and Inversion of the Stress Distribution in a Coal and Rock Mass with a Fault. *Int. J. Géoméch.* **2021**, *21*, 06021029. [CrossRef]
37. Zhang, B.H.; Hu, X.X.; Wang, Y.; Hu, Y.; Chen, W. In situ stress inversion and fracture characteristics around local fault in deep heterogeneous strata. *Pet. Sci. Technol.* **2022**, *42*, 448–469. [CrossRef]
38. Kou, H.; He, C.; Yang, W.B.; Wu, F.Y.; Nie, J.C.; Xie, J.C.; Fu, J.; Xiao, L.G. Distribution Characteristics of In Situ Stress Field for a Deep-Buried Tunnel in the Fault Area. *Int. J. Geomech.* **2023**, *23*, 04023074. [CrossRef]
39. Li, Z.L.; Wang, C.H.; Shan, R.L.; Yuan, H.H.; Zhao, Y.; Wei, Y.H. Study on the influence of the fault dip angle on the stress evolution and slip risk of normal faults in mining. *Bull. Eng. Geol. Environ.* **2021**, *80*, 3537–3551. [CrossRef]
40. He, H.J.; Su, S.R.; Mei, H.; Li, P. Numerical simulation of the mechanics of formation of a parallel reverse fault. *Arab. J. Geosci.* **2019**, *12*, 747. [CrossRef]

Disclaimer/Publisher's Note: The statements, opinions and data contained in all publications are solely those of the individual author(s) and contributor(s) and not of MDPI and/or the editor(s). MDPI and/or the editor(s) disclaim responsibility for any injury to people or property resulting from any ideas, methods, instructions or products referred to in the content.